FLUORESCENT PROPERTIES OF R6G-STAINED MOUSE BRAIN TISSUE

Sergio de Armas Rillo
Tutor: Dr. Fernando Lahoz Zamarro
ULL, Máster Universitario en Astrofísica

Julio de 2019

Contents

Resumen

La espectroscopía de fluorescencia es, desde el principio de su desarrollo, una de las disciplinas de la física con más aplicaciones multidisciplinares, resultando especialmente útil en investigación biológica, biomédica, química, en ciencia de materiales, etc. Su mecanismo es sencillo: mediante una fuente de luz (por ejemplo, un láser) se excita una molécula o átomo (que recibe el nombre de fluoróforo) presente en la muestra a analizar, promocionando electrones a niveles de energía superiores al fundamental (en el que se encuentra la mayor parte de la población de e^-). Estos electrones se acaban desexcitando mediante la emisión de fotones, emisión que podemos detectar. De la forma que tengan los espectros de absorción y emisión de las muestras podremos sacar abundante información acerca del fluoróforo, de su interacción con el medio y del medio en si.

En este trabajo se indujo fluorescencia en cortes transversales de cerebros de ratón mediante su tinción con un fluoróforo orgánico extrínseco, la rodamina 6G (R6G). Se escogió esta molécula, muy común en estudios de fluorescencia, por su alta eficiencia cuántica (es muy luminescente), su emisión y absorción en el visible, y por el gran conocimiento que se tiene de su comportamiento bajo distintas condiciones. Como todas las rodaminas, tiene también afinidad por medios lipídicos (como es el caso del tejido cerebral).

Se estudió la emisión de esta molécula al disolverse en agua y en etanol en varias concentraciones: de 1μM en agua a 50mM en EtOH. Acto seguido, se comprobó qué cambios sufría esta emisión cuando la R6G no estaba en disolución sino impregnando cerebros de ratón, habiendo sido estos bañados en las disoluciones estudiadas, concluyéndose que la R6G en disolución y la depositada en el tejido cerebral tenían comportamientos muy distintos: mientras que en el primer caso la mayor parte de la emisión era debida a las moléculas de R6G en su configuración habitual (monómeros), en el segundo caso la formación de agregados de mayor order, especialmente dímeros, hacía que fueran esto últimos los reponsables de la emisión, provocando en la misma un fuerte corrimiento al rojo.

Teniendo ya muestras de tejido cerebral fluorescentes y sabiendo cómo interpretar los espectros de R6G obtenidos, se procedió a realizar un mapeado de la fluorescencia de los cortes de cerebro de ratón, comparando muestras obtenidas de ratones sanos con aquellas provenientes de especímenes a los que se les había inducido Alzheimer. Se lograron fabricar mapeados de intensidad de emisión y de la relación entre la emisión en dos longitudes de onda determinadas, 615nm y 570nm, relación que sirve para caracterizar la anchura del espectro y el grado de dimerización de la R6G.

Acto seguido, se procedió a tratar de obtener, exitosamente, Random Laser en el tejido cerebral. El fenómeno de RL necesita de un medio de ganancia (proporcionado por la tinción de R6G) y la presencia de abundantes centros de *scattering*. Esta segunda condición

hace de los tejidos biológicos un medio muy favorable para la obtención de RL; sin embargo, hasta ahora no teníamos conocimiento de la aparición de este fenómeno en tejido cerebral. Se estudiaron las características pincipales del RL coherente obtenido (intensidad de emisión y threshold) atendiendo a las diferentes regiones cerebrales excitadas, y se encontró un comportamiento diferenciado del resto del cerebro en el cuerpo calloso. Por último, mediante análisis de Fourier,se logró determinar el tamaño típico de las cavidades resonantes que permiten el laseado.

Por último se construyeron interferómetros Fabry-Perot con el objetivo de mapear el índice de refracción del cerebro con alta resolución espacial. Tras la optimización en la fabricación de dichos interferómetros y un tratamiento intensivo de los datos se lograron estos mapas de n; sin embargo, se concluyó que hace falta un trabajo más exhaustivo para poder alcanzar datos suficientemente precisos de los que extraer conclusiones.

1 Theoretical introduction

1.1 Fluorescence Phenomena

When it comes to studying and analyzing nature, humans have always trusted, first and foremost, in light. Long time has passed since thinkers dedicated their times, and their eyes, to the passive observation of the world around us, yet light is still the best tool we have to further our knowledge. Of course, now we are not limited to what our eyes can see, and our understanding of the quantum nature of matter has allowed us to see light where there is none. With this I am refering to the phenomenon of luminescence: the emission of light derived from the transition of electrons from excited states to others of lower energy.

The luminescence of matter can be divided in two different categories: **fluorescence** and **phosphorescence**. The mechanism at play in both phenomena are different at the quantum level, althougth they are both manifestations of the aforementioned decay of electrons. When the excited and ground state of the electron share the same multiplicity (if we have spin **S**, the multiplicity is **2S+1**) the transition from the upper to the lower level produces fluorescence. If the multipicity is different, then the transition is forbidden under electrical dipole moment matter-radiation interactions and we have phosphorescence. Usually, the former happens with **singlet -singlet** transitions, where bot states have spin 0 and multiplicity 1, whereas the latter appears in **triplet-singlet** transitions. A good way of visualizing this fenomena is the Jablonski diagram, in which the energy levels and possible transitions are shown. One example can be found in figure 1.1.

But this distintion would not make sense if there were not ways of distinguishing between both in a macroscopical level. Mainly, we discern Fluorescence from phosphorescence from the lifetimes of emission (althougt the quantum yields of the luminescence are also significantly different). We will define both concepts just below this introduction, but let us say for now that fluorescence presents average lifetimes of around 0.1-10 ns, while phosphorescence, steeming from a forbidden transition, has lifetimes significantly longer, from 1ms up to 10s and even longer (page 456 in [2]).

In order to study biological systems it is more convenient to use fluorescent molecules (fluorophores) instead of phosphorescent ones. Fluorescence is easier to detect, has a lifetime comparable with the timescales of many

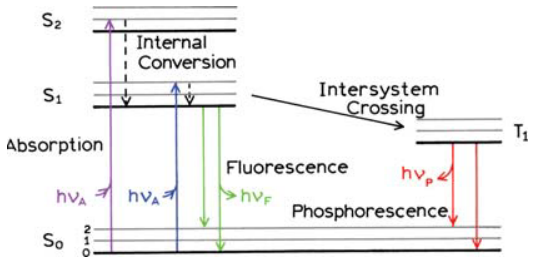

Figure 1.1: We can see the fundamental level $\mathbf{S_0}$, two excited singlet levels ($\mathbf{S_1}$ and $\mathbf{S_2}$) with their respective vibrational levels and a triplet state $\mathbf{T_1}$ from which phosphorescence originates. Image extracted from [1].

microbiological processes, can be easily observed at room temperature, has a higher quantum yield... This is why a flourophore has been chosen as dye for this work. It is useful to list some of the common characteristics of fluorescence [1] that we may have to keep in mind when analysing the obtained experimental results.

- **Stokes Shift**: Flourophores do not absorb and emit at the same wavelengths, as can be seen in figure 1.2. When we promote an electron to a higher enery level, it rarely ends up in the ground vibrational level associated with this new orbit. Then, non-radiationally, it decays to the ground vibrational level from which it jumps bak to the lower energy state by the emission of a photon that is, obviously, less energetic than the one that excited the electron. Aditionally, the decayed electron does not have to fall to the ground vibrational level of the lower-energy state from where it jumped, which further increases the difference between energy absorved and energy emitted. All fluorophores share this shift, in some cases less dramatically than others, and characteristics of the medium can alter it, giving us information about the state of the emitting molecule. Stokes shift can be altered because of energy transfer, excited-state reactions, **complex formation**, and solvent effects [1].

- **Emission spectra independent from the excitation wavelength**: even though we can promote the electron to a variety of excited states, it is very common that the emission only takes place between two clearly defined states (lets call them $\mathbf{S_0}$ and $\mathbf{S_1}$), one being the ground state and the other a metastable excited level. The desexcitation from whichever vibrational state the electron was promoted to, to the lowest vibratonal level is very fast, of the order of picoseconds. Therefore, we do not expect significant changes in the emission of the dye when using different instruments that do not share the same excitation lasers.

- **Fluorescence lifetime and quantum yield**: "quantum yield is the number of emitted photons relative to the number of absorbed photons" [1]. The higher the quantum yield, the brighter the emission of

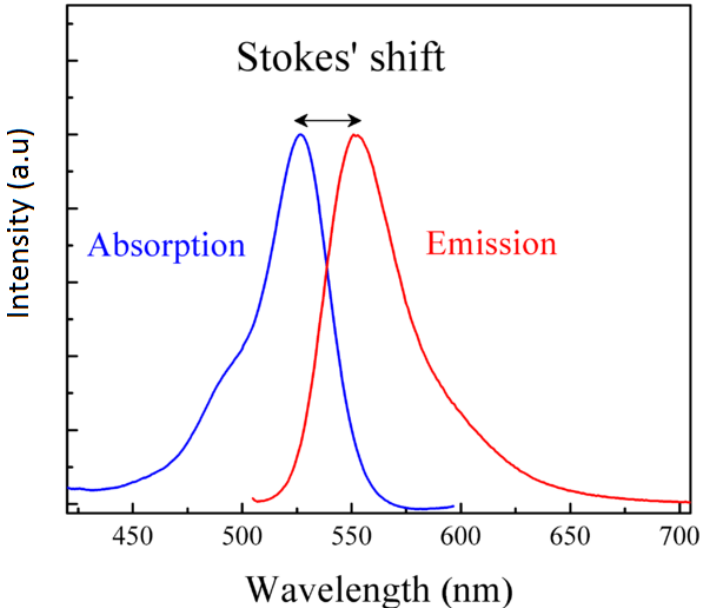

Figure 1.2: Absorption and emission of R6G. Extracted from [4]

the flourophore. A high quantum yield means that there are few and inefficient non-radiative decay paths for the electrons. Other aspects that affect quantum yield are the interactions with the media, the formation of aggregates, resonance energy transfer...

Lifetime is defined as the average time that the electron spends in its excited state before emission. If Γ is the rate of emission of the fluorophore and k_{nr} the rate of non-radiative decay, we can write:

$$\tau = \frac{1}{\Gamma + k_{nr}}$$

The natural lifetime is the lifetime if there was not any non-radiative decays, so $\tau_n = 1/\Gamma$. We can also define the quantum yield using these rates:

$$Q = \frac{\Gamma}{\Gamma + k_{nr}}$$

Therefore:

$$\tau_n = \frac{\tau}{Q}$$

We can infer properties of the medium and the state of the fluorophore studying τ

- **Fluorescence quenching**: when the emission of the fluorescence is dampened, we are talking about quenching. There are many ways quenching can appear: collisional quenching, where the interaction between the excited fluorophore and the medium desexcites the former

without photon emission; formation of complexes with quenchers; self-aggregation, forming non-emitting complexes; even a high absorption rate of the fluorophore can quench the total emission of a sample.

- **Steady-state and Time Resolved fluorescence**: In the first type of measurements (the most common ones), the observation and the excitation of the sample happens simultaneously. After we incide on the sample with an excitation beam (a laser, light coming from a monochromator...) the emission starts almost inmediately, so the steady state is reached with ease.

  Time-resolved measurements are obtained using a single, very brief pulse of light, that can be considered instantaneus compared to the lifetime of the fluorescence at play. After the excitation of the sample we need to detect the emission of it at a very high speed to see how the decay of the excited electrons behaves with time. Steady-state measurements are nothing but the average of time-resolved behaviour of the molecule over its intensity decay. There is a proportional correlation between longer lifetimes and higher intensities in steady-state measurements.

- **Intrinsic and extrinsic flourophores**: we can distinguish between two types of fluorophores. Intrinsic ones are those molecules that are already present in the studied sample and naturally exhibit fluorescent behaviour under certain circunstances. An example would be the tyrosine, an aromatic amino-acid present in many proteins. However, many times we do not have fluorescent behaviour in our sample, so we have to resort to the use of extrinsic fluorophores: fluorescent molecules added to the sample. Brain tissue, with its highly lipidic composition, does not produce fluorescence. That is the reason why we have needed to dye the samples with an extrinsic fluorophore, Rhodamine 6G.

Having presented the main properties of fluorescence related to this work, it is time now to introduce the fluorophore used in the experiments, the reasons for its use and its particularities.

1.1.1 Rhodamine 6G

Rhodamines are used mainly because they are excelent fluorophores: quantum yields that approach unity. But this is not enough to justify its use ahead of the huge number of fluorescent dyes present in the market. Leaving aside more mundane considerations, such as its not-so-high pricetag, we can find that they happen to be excellent extrinsic fluorophores for lipidic mediums, such as the brain tissue (chapter 3 in [1]). Both absorption and emission occur in the visible spectrum (green for the first and orange for the second), which will facilitate the experiments. The emission also occurs far away from

the wavelengths at which proteins' fluorescent components emit, so we will be able to identify the emission spectra with the R6G without ambiguities.

Rhodamine 6G (formula $C_{28}H_{34}ClN_2O_3$) has the structure ilustrated in figure 2.1, where we can clearly see the aromatic elements from which fluorescence arises. This fluorophore absorbs in the green ($\sim 552nm$) and emits in the orange region of the spectrum (peak around $575 - 590nm$). Figure 1.2 illustrates both spectrums for R6G in dilution (this molecule is very solvent in EtOH, although we can reach concentrations above 10mM of R6G in water).

However, this emission and absorption can experiment significant changes depending on the specific conditions under which the R6 molecules are present. In general, when aumenting the concentration of rhodamine we see two main effects: one is the quenching of the emission, due both to a higher extintion of the excitation light (the higher concentration of fluorophres means that there will be a bigger absorbtion) and because R6G starts to self-aggregate, forming dimer, trimers and even higher-order complexes that produce much less (or not at all) fluorescence. The formation of these higher order complexes also directly affects the shape and location of the spectrum. We see a clear redshift and the formation of a shoulder in the absorption spectrum [6], both due to the presence of R6G dimers [7] [8]. In this case, emission is dominated by J-dimers, while the shoulder in absorption is due to the non-emissive H-dimers. Wherever we have higher concentrations of R6G, or a bigger surface on which to deposit, we expect to see a broader, redshifted emission spectrum.

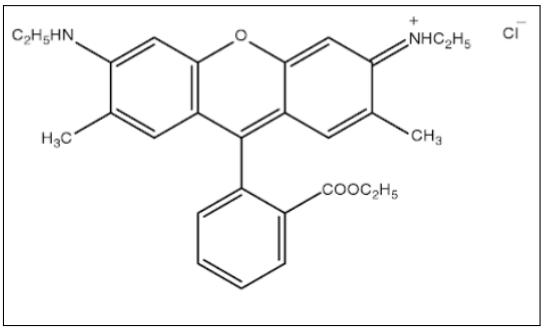

Figure 1.3: R6G molecule. Extracted from [5]

1.2 Random Laser

The phenomenon of random laser (RL from now on) has only recently picked up attention, althougth its fundamental physics were theorized as early as the 1960s by Lethokov. It is an example of light difussion in materials with amplification (gain) [3]. The physics of RL is very complicated, as it implicates diffusion and scattering of light in a disordered medium, interference, coherence, formation of different modes, the nature of the gain of the medium, a chaotic behaviour in certain regimes that produce a non-gaussian intensity distribution (specifically, a Levy distribution [3])... However, we can summarize the phenomenon: when we have an optically thick medium with gain and scattering centers (the more, the merrier), there is the possibility that the diffused incident light, following a random path through said material, ends up following a closed optical path where the gains exceed the

losses, stimulated emission is produced and laser emission is obtained. For this to happen we need the excitation beam to present a high energy density (there is an energy threshold below which RL does not happen), it must come in the form of a brief pulse (specially for energies around the threshold).

We can differentiate betwen two types of RL emission: incoherent and coherent. The first one is characterised by a narrowing of the emission band, with a FWHM of about 10-15nm, and a nonlinear relation between the excitation intensity and that of the emission [9]. The second one, that happens when the light is able to form closed optical paths in the medium, presents a series of small, narrow peaks (typical FWHM of 1nm), each one associated with a different mode (that is, in time, associated to a different optic loop) [9]. If we have coherent RL we can obtain the sizes of these paths and obtain information about the geometry of the tissue performing Fourier analysis of the obtained RL spectra. Without indulging in the math, we find that the Fourier modes follow this expression:

$$p_m = m\frac{L_C n}{\pi} \tag{1.1}$$

Where p is the mode (chosing the appropiate sample units p is measured in λ), m is the order, n is the refractive index of the medium and L_C is the size of the cavity where the lasing happened.

1.3 Fabry-Perot Cavities

When talking about a Fabry-Perot cavity what we have to picture is a Fabry-Perot interferometer, or etalon. It consists on two reflective surfaces opposite and parallel to one another: the space between them is what we have come to call "Fabry-Perot cavity". When light enters this space, it becomes trapped inside the cavity thanks to the mirrors, and starts suffering succesive reflections. As can be expected, interference arises and when eventually a beam of light escapes the etalon it presents a superimposed pattern in its spectrum. A certain wavelength (in fact, wavelength**s** because we are dealing with equally prominent modes) have the proper size to suffer constructive interference and appear as spikes in the normal spectrum. These local maxima follow pretty closely this equation:

$$m\lambda_m = 2nd \tag{1.2}$$

n is, again, the refractive index inside the cavity, while d represents its width. If we know one of these two parameters we can determine the other if we somehow approximate m, the order of the peak. For that we can take advantage of the free spectral range, FSR:

$$FSR = |\lambda_{m-1} - \lambda_m| = \frac{\lambda_m}{2nd} \tag{1.3}$$

With both relations we expect to obtain a mapping of the refractive index of the brain, after some data manipulation. For a more detailed description of the Fabry-Perot interferometer, with a more in-deep determination of the regimes where both expressions hold true, see [2]. chapters 2 and 9.

1.4 Objectives

With the concepts at play being presented, we now want to apply them to the concrete situation of studying a biological sample: brain tissue. It goes without saying the capital importance that the study of this organ has adquired lately, and there is a need for different and novel ways of accessing its inner workings. With biology being a science more and more open to a multidisciplinary approach it is interesting to apply the techniques and notions described so far to the study of the brain. This study has been performed using three different approaches: first, fluorescence measurements, then RL obtention and finally analysis of the brain inside a F-P cavity. The fluorescence will give us information about where is located the dye with more concentration, and also in what manner it is present (monomers or higher-order aggregates?): we hope that we will find differences between healthy brain tissue and BT of mice with Alzheimer's disease; RL will give us information about the scattering strength of different parts of the brain, and the Fourier analysis of said RL can tell us about the spatial conformation of the tissue in certain zones; finally, F-P data will be used to determine n inside the brain.

2 Methodology

Althougth subjected to three different types of measurements, the samples have suffered essentially the same preparation. Most of the equipment is shared too, and the main differences come at the data analysis performed in each case. The obtention and preparation of the samples were carried on by the team of Ángel Acebes in the *Departamento de Ciencias Médicas Básicas, Instituto de Tecnologías Biomédicas* at ULL up to the point of brain dyeing, at which point I took over.

2.1 Brain Tissue Handling and dyeing

As seen in [10]: *The experiments were carried out on C57BL/6 male mice (n=6). Experimental protocols were approved by the Ethical committee of the University of La Laguna (Reference # CEIBA2013-0083), and are in accordance with the European Communities Council Directive of 22 September 2010 (2010/63/EU). Mice were deeply anesthetized with an overdose of sodium pentobarbital and transcardially perfused with heparinized ice-cold 0.9% saline (30 ml) followed by 4% paraformaldehyde in phosphate buffered saline pH 7.4 (PBS, 50 ml). Brains were removed and stored overnight in the same fixative at 4°C. Then they were cryoprotected in sucrose 30% in PBS and stored at -80°C until processing. Coronal sections (100 µm) were obtained with a freezing microtome and collected in 6 parallel series.*

The coronal sections were sent to the *Departamento de Física, IUdEA* where some were stored in a commercial fridge, at a temperature of 4°C, while others were stored in a ultrafreezer at -80°C. The firsts were used for the first round of fluorescence experiments and its mapping. The rest, better conserved, were the ones employed in the RL and F-P experiments.

The brains were dyed inmediately before the experiments were carried away, first eliminating the sucrose medium in which the lingered on, substituting it with different R6G dilutions: R6G/PBS and R6G/EtOH at a range of concentrations. For the fluorescence measurements, as we did not count with any protocols in place, different samples remained for different times in the bath, ranging from a day to as little as 15 minutes. RL experiments where conducted on samples that had remained for one hour in a bath of R6G/EtOH at these concentrations: 5mM, 10mM, 20mM and 50mM. Not

all the brains samples that ended up inside the F-P cavity were dyed, as we found that they gave the best signal when not tinted wit the fluorophore.

2.2 Obtention of luminosity and Fabry-Perot inteferometry mappings

For both fluorescence mappings and F-P mappings a Renishaw inVia confocal microscope was employed, using a 532nm laser for excitation and a motorized, programmable holder. This instrument generates steady-state spectrums. For time-resolved emission spectra, necessary for the characterization of the emission of R6G, an Edimburgh Instruments LifeSpec II fluorescence spectrometer was used, equipped with a multichannel plate photomultiplier (single photon counting) for photon detection. Excitation of the sample was possible thanks to a Edinburgh Instruments EPL-470 picosecond pulsed 470nm diode laser. It generated pulses with a temporal width at half maximum of 80ps, while generating an order of 10^6 pulses per second. The software used for the control of the instruments, obtention of data and lifetime estimation were Edinburgh Instruments F9000 adquisition- and FAST software (the later one, with a temporal resolution of 0.3ns, allowed the obtention of the lifetimes of the samples via reconvolution of the instrument response function).

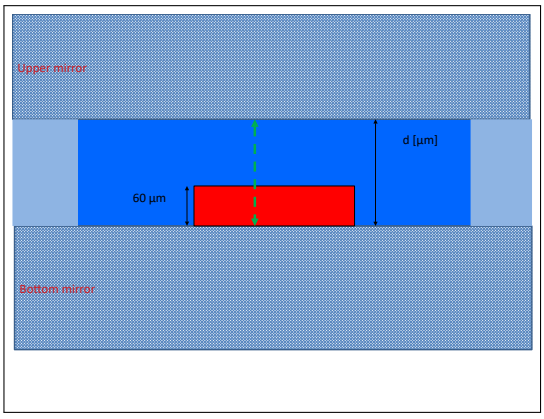

Figure 2.1: Blueprint of the built Fabry-Perot resonator

The mappings were possible thanks to the ability of the Renishaw inVia Raman microscope of accepting a 2D pattern to sample an extended region. Using a python script to stich together the huge amount of spectrums obtained in each mapping (around two thousand), it was possible to analize the entire brain at once, both for its luminosity and Fabry-Perot behaviour. For the fist measurements, the obtained emissions where smoothed, its intensity obtained by integration of the spectrum, its maximum and broadening determined, all to generate the images we will see in the next chapter. The F-P data was, on paper, as easy to treat once we had a method of creating the images as the fluorescence data. However, it probed to be more difficult to treat, mainly because the significant noise incurred when the incident beam arrived at the brain tissue, difficulting the detection of the superimposed periodical signal associated with the constructive interference. We will illustrate this problem in the next

chapter too.

It is important to describe the actual shape of the F-P cavity. Two thin plastic sheets, both one-sided mirrors. where placed opposite to one another. One of them had a built-in separator that ensured the formation of a $170\mu m$ deep cavity in which we put the BT samples. Different ways of obtaining some gain inside the cavity were used: directly staining the brain, using stained brains with a drop of R6G/EtOH, PBS or glycerol, and using non-dyed samples inmersed in a drop of R6G/PBS and R6G/glycerol. Without this gain it would be impossible to detect any light whatsoever.

2.3 RL measurements

For the RL measurements we needed a pulsed laser. A Nd-YAG one, emitting pulses (8ns long) of light with $\lambda = 532nm$, was used. It had a rate of shooting of 10Hz. Then a custom experimental setup was necessary to ensure that the beam would incide properly on the sample. The beam was homogeneized using a pinhole just as it exited the laser, and two linear polarizers allowed us to modulate the intensity of the beam. As we had to avoid hitting the sample with a continuous beam, a camera shutter was used. Each shot arrived focused and normal to the sample thanks to a cylindrical lens, and in the form of a horizontal line with a size of 2.5x0.5mm.The emission of the sample was collected at an angle of 30º from the normal, using a convergent lens to capture a biger amount of radiatiion. Through an optic fiber the signal arrived to a CCD spectrometer with a top spectral resolution of 0.05nm. The experimental setup is outlined in figure 2.2

For RL the samples had to be left in contact with air, without a cover, but apart from that the preparation and handling of BT sections was identical to the previous luminescence measurements. The search for the RL threshold was possible thanks to the use of an oscillocope and a detector, that allowed us to determine the intensity of the radiation before shooting at the sample.

With the obtained spectra a PFT analysis was conducted, using the Origin Pro 7 software, but having to determine by hand each Fourier mode.

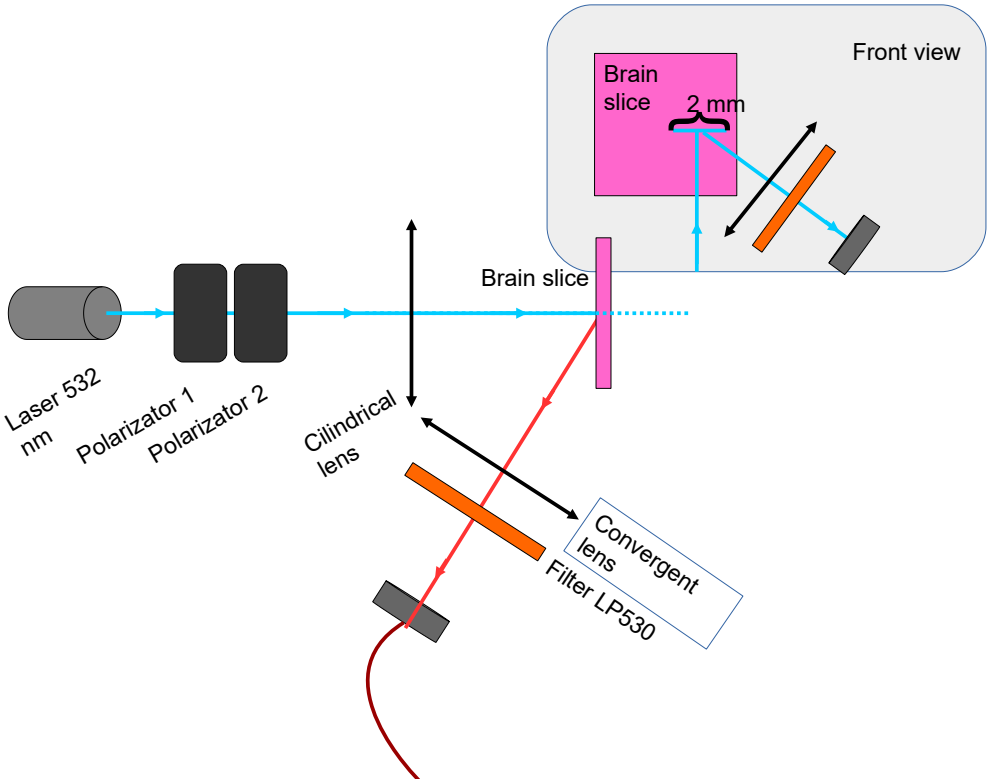

Figure 2.2: Both polarizers are used to regulate the intensity of the incident beam: if perpendicular, no light reaches the brain; if parallel, the full laser output will hit the sample. The angle of detection was around 30º.

3 Results and discussion

Let us remember what were the main objectives of this master's thesis:

- **Fluorescence measurements**: obtention of the spatial distribution of emission intensity and spectral broadening in the dyed brain tissue. Search for differences between healthy brains and the ones suffering from Alzheimer's disease.
- **Random Laser**: to produce random lasing in the biological tissue. To study it characteristics (threshold, coherence and modes through PFT analysis) depending on the excited region
- **Fabry-Perot cavities**: to determine the refractive index of the brain using an etalon.

The first and last points drive us to the obtention of mappings of the brain, as was seen in the previous section. But before that it was necessary to specify the emission spectrum of the used dye, both suspended in dilution and once deposited on the brain. In figure 3.1 we can see the emission spectra of four dilutions of R6G in ethanol, each one at a different concentration: 5mM, 10mM, 20mM and 50mM; they were obtained in different conditions. The first emission spectrum was obtained directly from the solutions. Then the brains were stained and the other three measurements were performed: a steady-state spectrum, a time-resolved one at t = 0ns (the moment of the excitation) and another one at t = 9ns. R6G has a lifetime of around 4ns, so this last one spectrum is expected to be much more noisier than the rest.

The spectra in the image are normalized, but the emission was heavily quenched when we went from lowest to highest concentration. However, neither the peak of the emission (at 565nm) nor the FWHM (34-38nm) suffered significant changes. This means that whatever dominated the emission in the 5mM dilution was still responsible for the luminosity of the 50mM one. But why the quenching then? Well, for starters, with a higher concentration of the fluorophore it is inevitable that we find higher absorption. Even more for rhodamines, that have a very high molar extintion coefficient, around $8 \cdot 10^4 M^{-1} cm^{-1}$. But also the formation of higher order aggregates can produce quenching. When we increase the concentration, R6G molecules are going to self-aggregate [11], and it can happen that the excited monomers, instead of decaying to their ground state, transfer their energy through the

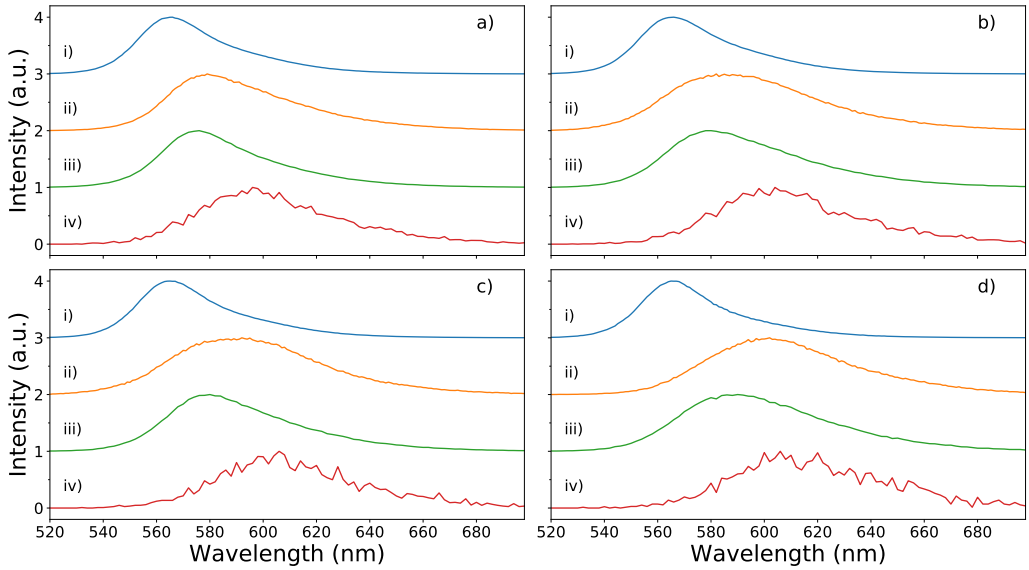

Figure 3.1: Clockwise from top left, we have **a)** 5, **b)** 10, **c)** 20 and **d)** 50mM. In each panel, i), ii), iii) and iv) signals, repectively: R6G/EtOH dilution, steady-state spectrum of the stained brain, the spectrum at t = 0ns and at t = 9ns

aptly-named procces *energy transfer* to an aggregate in its ground state [12]. This transfered energy will not produce light and will therefore not be there for us to see, quenching the emission of the dilution. Therefore, we conclude that the emission seen in the dilutions is due to monomers of R6G, and it is quenched by the formation of aggregates of said fluorophore when we increase its concentration.

Now, when we dye the brains, R6G is deposited in its surface, invading the crevises and irregularities that a biological tissue is going to have. Once deposited the formation of aggregates is increased, specially dimers. We see that, inmediately upon staining the brains, the spectrum suffers a noticeable redshift and broadening. What we have now is a mix of monomers, J and H dimers and higher order aggregates: not only from the interaction between R6G monomers and the brain surface, but also because the sample, while still damp, is not inmersed in liquid. The drying tissue contributes to the precipitation of R6G. The first two (monomers and J-dimers) are luminescent, with the fluorescence of the dimers being less energetic. Aggregates of more than three molecules of R6G tend to have very poor fluorescence, and H-dimers are also non-luminescent. The number of dimers is now comparable to the number of monomers, and given than monomers tend to transfer energy to the dimers it is not far-fetched to assert that the emission of the stained brains is mainly due to J-dimers. The rest of the somewhat emitting combinations of R6G molecules contribute to the broadening of the spectrum, which is also far more dim that the one we find in R6G/EtOH dilutions. The most dramatic change of the spectrum can be seen in the sample stained with

50mM dilution, as would be expected.

When we go to the time-resolved spectroscopy we see that, inmediately after the exciting pulse, the emission is lightly blueshifted and sharpened in comparison to the steady-state one. We still have a long tail and a significant redshift from the monomer spectrum. This means that at this point of time the emission is even more dominated by the dimers, with the monomers that get to emit before suffering a non-radiative decay because of the presence of higher-order aggregates having an important role still. When we go to t=9ns the picture is completely different. Although the signal is much noisier, it is clear that now we do not have dimer or monomer emission. Only the higher order aggregates are still excited and capable of fluorescence. The timeline is as follows: inmediately after excitation, monomers, with the excited state of the molecule having a short lifetime, rapidly start emitting. However there is a competing desexciting path: the energy transfer to dimers (and polymers beyond those). J-dimers not only emit, but also do so with lifetimes comparable to that of monomers. So J-dimers emit at the same time as the monomers, and those monomers that stay excited for too long transfer their energy to the dimers, quickly quenching the monomer emission. J-type dimers decay in a short time, and only those higher-order aggregates with very low quantum yields (and also high lifetimes) keep on emitting once we reach t = 10ns.

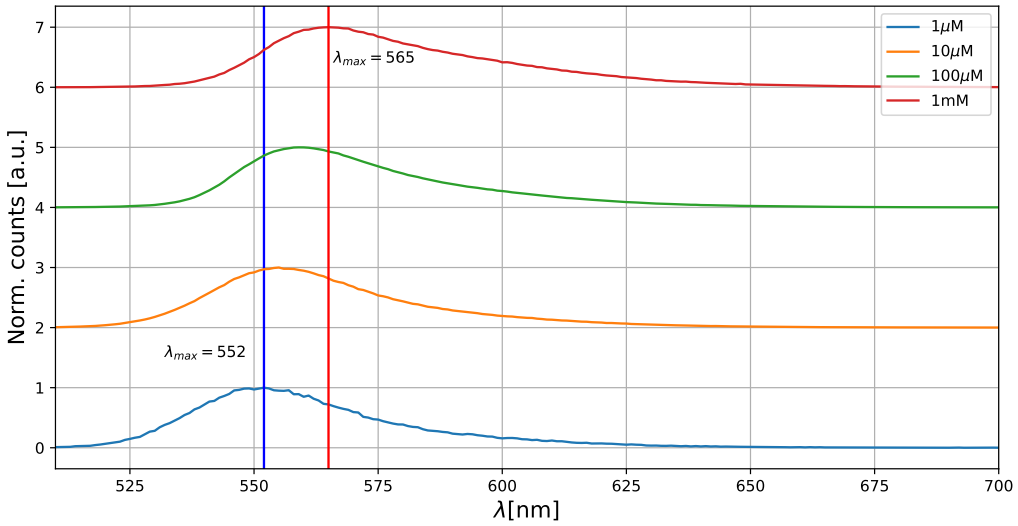

Figure 3.2: The peak wavelength is marked for the lowest ($1\mu M$) and highest (1mM) concentrations

It is interesting to see what happens with R6G/PBS dilutions, which were also used for the fluorescence mappings. Those dilutions reach a lower maximun concentration, as R6G is less soluble in water than in EtOH. The concentrations of those dilutions were $1\mu M, 10\mu M, 100\mu M$ and 1mM. A dilution of concentration 10mM was also used to stain the bains, but in the obtention

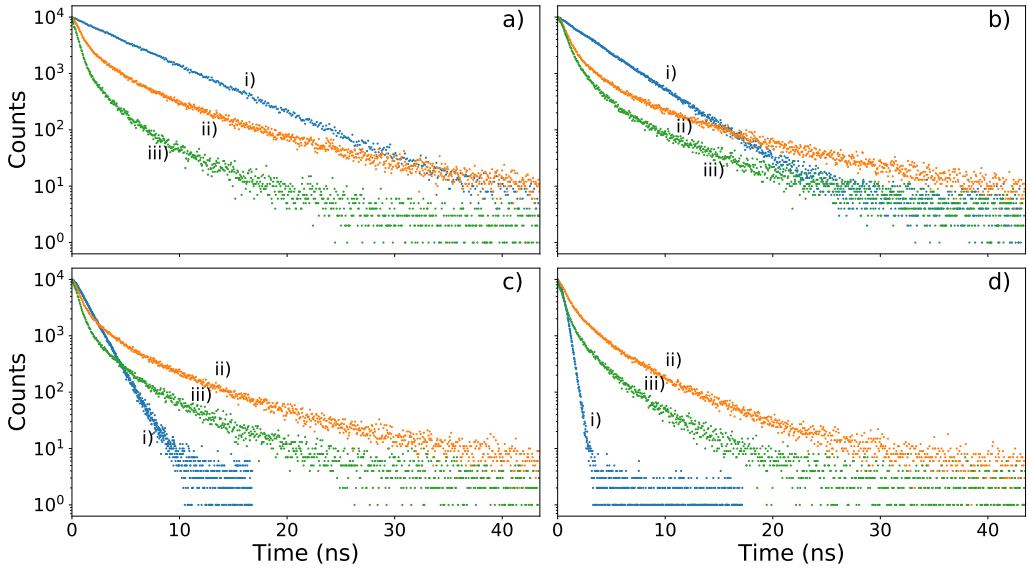

Figure 3.3: Same disposition of concentrations as in fig. 3.1. i) shows the decay at 565nm in the dilution; ii) and iii) come from the stained brains and correspond to 620 and 580 nm.

of the emission spectrum of said dilution re-absorbance effects made it difficult to obtain a good enough signal. The emission spectra of said dilutions can be seen in fig. 3.2.

Now it would be a good time to study the decay of the emission on the samples, hoping to directly determine the lifetimes of the emitting compounds. Once again we work with the same 4 different concentrations of a dilution of R6G in EtOH. We will detect the decay in intensity in one wavelength in the case of the dilutions (565nm) and two in the case of the brains: 620 and 580 nm. For the dilutions we only have one important contributor to the emission and that is why we only analyze the decay in one wavelength. For the stained brains we have both dimer emission and higher-order aggregates emission, that lasts much longer, and that is why we focus on a wavelength associated with each type of fluorophore. We can see the decay curves in figure 3.3.

The intensity decays of the fluorescence of the dye solutions showed an exponential behavior and could be fitted to the expression:

$$I(t) = Ae^{\frac{-t}{\tau}} \tag{3.1}$$

Where A represents the intensity at t = 0 ns, and τ means the decay constant of the excited level. The value of τ was 5.0 ns for the 5 mM R6G/EtOH solution and decreased at 3.3, 1.2, and 0.4ns as the concentration increased to 10, 20 and 50 mM, respectively. The reduction of τ as the dye concentration increases happens because with higher concentrations we have higher number of aggregates to which transfer energy, resulting on an overall decrease of

Conc.	λ_{em} $(\pm 0.5nm)$	FWHM $(\pm 1nm)$	$\tau(\pm 0.1ns)$	$\tau_{av}(\pm 0.2ns)$ at 580nm	$\tau_{av}(\pm 0.2ns)$ at 620nm
5mM	566	37	5.0		
10mM	566	38	3.3		
20mM	565	36	1.2		
50mM	565	34	0.4		
5mM	579	50		0.8	2.9
10mM	582	63		1.6	2.8
20mM	592	63		1.3	2.3
50mM	602	60		1.1	2.3

Table 3.1: Main features of the emission spectrum and lifetimes of the R6G in dilutions (colored in orange) and stained brains

the emission with time(the energy goes to the ground state of non-radiative aggregates, that will not contribute to the emission). The drop of τ in the solutions was accompanied by a quenching of the emission intensity, as we saw just before.

Now, we know that the brain samples are impregnated by several types of aggregates that transfer energy to each other and to the medium itself [13]. It is not a surprise then to find that the decay curve is not a simple exponential. For the fitting of this curve three different exponentials were necessary, forming a multi-exponential decay:

$$I(t) = A_1 e^{\frac{-t}{\tau_1}} + A_2 e^{\frac{-t}{\tau_2}} + A_3 e^{\frac{-t}{\tau_3}} \tag{3.2}$$

Each A_i, τ_i represents the same as it represented in the case of the simple exponential decay, but associated to each contributor to the decay of the intensity. We can define an average lifetime:

$$\tau_{av} = \frac{A_1\tau_1^2 + A_2\tau_2^2 + A_3\tau_3^2}{A_1\tau_1 + A_2\tau_2 + A_3\tau_3} \tag{3.3}$$

On average the lifetime of the excited molecules that emitted at 580nm was shorter (0.8-1.6ns) that the one for the molecules that dominated the emission at 620nm (2.3-2.8ns). Given that the later is associated with the higher-order aggregates while the former comes from dimers we find an agreement with the analysis we made of the time-resolved spectroscopy. The results of the study of the sprectrums and decay curves of these different samples are summarised in table 3.1.

3.1 Fluorescence mappings

Having determined the behavior of R6G in our samples, we now proceed to map said intensity along the entire surface of a transversal section of a

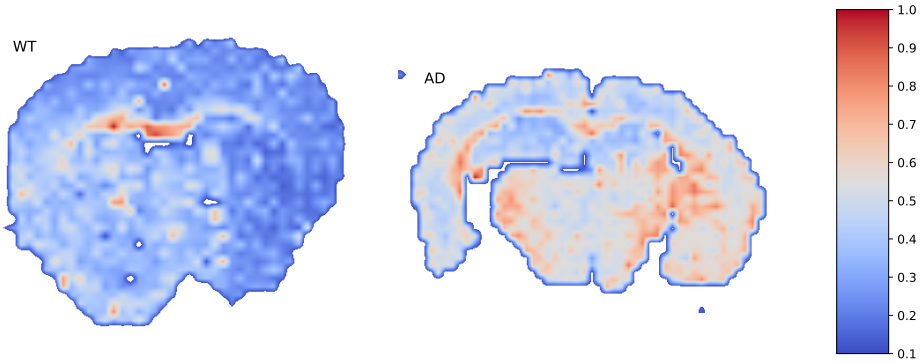

Figure 3.4: On the left, marked with **WT**, we have the mapped normalized intensity of emission of a sample of healthy brain tissue. On the left we see the brain of another mouse, brother of the former, who was induced to develop Alzheimer's disease (**AD**). Both mice are then from the same genetic lineage. Measurements were taken every $100\mu m$, covering a surface of roughly 5x3mm. **Both brains remained in a bath of R6G/PBS 1mM for 20 hours**

mouse brain. As has been said, the main goal of this analysis is to find significative differences between the luminescence of healthy brains (Wild Type brains) and those suffering from Alzheimer's disease (AD brains). The reason why we expect to find a difference is twofold: on the one hand, AD produces physical injuries in the organ, that can be seen even in CT (Computed Tomography) and MRI (Magnetic Resonance Imaging) scans [17] [18] in sufficiently advanced states of the illness. We expect those changes to be gradual, and therefore would be present in a smaller scale earlier, when the brain is less affected. If we have a more porous brain that has lost some amount of mass it could be possible to find that surface effects have promoted the accumulation R6G and formation of dimers. In the second hand, rhodamines have a high affinity to amyloid fibrils [14], which is very interesting when studying Alzheimer's disease. One of the main indicators of AD is the aboundant presence of the protein β-amyloid. It is possible that the build-up of said protein can affect the distribution of R6G concentration and therefore the fluorescence from the brain.

We see in fig. 3.4 that, in general, the emission in the diseased brain is closer to its peak value among the entire brain. The total intensity was calculated by integration of the fluorescence spectrum in each point. The peak intesity in the case of the WT mouse was found to be $5.74 \cdot 10^6$ counts and, for the one with AD, $6.76 \cdot 10^6$ counts (both in arbitrary units). In general the intensities were similar, but we saw the total emission was different depending in R6G concentration and aggregation. So, why not study directly the total emission intensity?

The main reason is that we are more interested in the distribution of said intensity than in the global value. The effect we expect to see from the existence of AD are not drastic enough to provoke a brain-wide change, at least not at the stage of the disease the mice presented when euthanized. Apart from that, the manipulation of the samples did not follow a protocol as strict as is usual in biomedical research, so the spectral adquisition sometimes differed between samples (excitation pulse, measurement time...). Not only that, but different dye concentrations, dye solvents, and staining bath were used during this stage of the study, as the optimal treatment for the brains was yet being determined. Although these differences were minimized and eventually when comparing brothers (as was this particular case), the search for generalized differences among all samples asked for the study of only normalized data.

Having clarified why total intensity is not analyzed, figure 3.4 has to be described. As was said earlier, high values of fluorescence are more generalized in the AD brain. In both samples we find a very emissive region, that is identified as *Corpus Callosum*. This region of the brain interconnects both hemispheres and consists mainly on axons, almost void of neuron bodies. Axons are covered and protected by myelin (produced by neuroglia), a lipidic substance. This means that the *Corpus Callosum* forms a very lipidic environment. Rhodamines are very lipophilic, which explains the concentration of the fluorophores in this region. Since the staining dilution had a low concentration (1mM) we don't expect to see a high amount of higher-order aggregates, even taking into account surface effects. The emission is dominated by monomers, which means that higer concentrations of R6G will increase the luminosity instead of quenching it. This is a different situation than the one seen in the last section with concentrated R6G/EtOH dilutions, and the individual spectrums (an example of them would be figure 3.5) are more similar to the ones seen in figure 3.1.

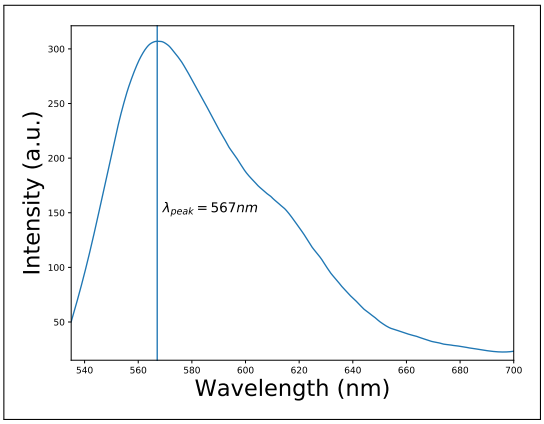

Figure 3.5: Example of emission spectrum of the AD brain. The position of the peak indicates that the dominant fluorophores are R6G monomers. However, the presence of the shoulder in the spectrum tells us that there has been a crtain degree of aggregation and there are J-type dimer emitting.

So we see that in both brains the emission occurs mainly in the *Corpus Callosum* region, but it is more widespread in the AD brain. Could this be because a hypothetical increase of irregularities on the surface of the cut, product of the loss of mass of the brain, or the early build-up of β-amyloid?. Both explanations are possible, but it would be impossible to tell with just two samples.

Emission intensity is linked, in this case, with a higher concentration of R6G monomers. However, that does not mean that there is no dimer

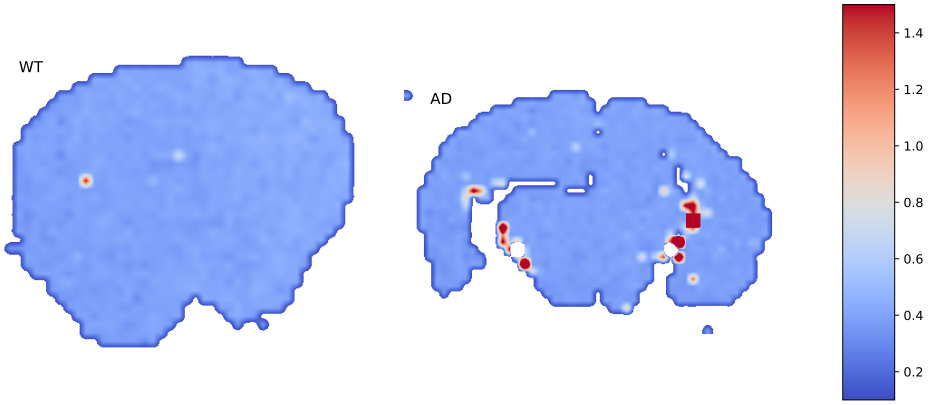

Figure 3.6: These are the same samples as in figure 3.4, but now the ratio I_{615}/I_{570} is mapped. Ratios greater than 1.5 and lower than 0.1 are masked

formation. In this case of significant monomer domination we can use as a test of aggregation the redshift and width of the spectrum. Wider and redshifted spectra indicates the presence of J-dimers, and we can test both by analizing the ratio of intensity between two different wavelengths: 570nm (near the monomer peak) and 615nm (this λ associated to dimers). We can see the result of mapping this ratio I_{615}/I_{570} in figure 3.6.

The emission of the brain is fairly homogeneous in regards to its width, and does not suffer from noticeable redshifts. The value of the ratio in most points of both brains is 0.3-0.4. This indicates that there has not been significant dimer formation. Th samples are covered, so it could be possible that this cover had preserved a humid environment, but since the mapping takes a long time (from 45 minutes for very emissive samples to more than 4 hours, depending also in the resolution of the sampling) this is not a satisfactory explanation for the lack of aggregates. A more reasoble one is that the aggregation proccess that shaped the emission seen in 3.1 happens before staining the brain. The formation of a thin film then facilitates the energy transfer between monomers and the rest of R6G polymers (whose formation is also promoted by the drying sample). It is worth noting that the measurements of fig. 3.1 were performed on uncovered brain slices.

So far we have analyzed the luminescence from a pair of brains. But it is impossible to draw any conclusions from just two datasets. A total of 8 different brain slices were mapped. The first one was heavily damaged after manipulation and was used to test the experimental technique and to practice the handling of such delicate samples. Of the other seven: two (from the same litter) were bathed for 20 h with 10mM R6G/PBS; another one was stained by the same dilution but stayed for 4 more hours; other two, with 1mM of the

same dilution (those are the ones showed in figures 3.4 and 3.6) during 20h, one was dyed with 50mM R6G/EtOH during 18h; lastly, one was tinted after spending an hour in the solution R6G/PBS 10mM, but was then inmersed in a custom-made cubet of PBS for the duration of the measurements, hoping to keep the brain wet.

We point out those diferences because there was hardly any common luminescent behaviour among all the brains. The only almost consistent finding was a higher fluorescence intensity and/or I_{615}/I_{570} ratio in the *corpus callosum*. However, ''almost" is not used lightly: we found exceptions to this in some of the only 8 measurements made. In annex A we present all the obtained mappings to show the lack of consistency in the results. There are plenty of possible explanations for this negative result: the brains were not properly conserved (they were stored at 4ºC when they should have been kept at -80ºC to ensure proper conservation), and that degraded the biological samples. Given that the different measurements were separated in time, sometimes even for weeks, the degradation was not the same in each brain. The staining bath was not only different for almost each sample, but also could have affected the staining itself: at the beggining there was not an special care to avoid the folding of the slices, which could cause an uneven impregnation of R6G. The orientation of the recipient in which the bath took place could also affect the staining: in one sample there was an unmistakeable top-bottom gradient of intensity that can be a gravity effect. Different staining dilutions also meant that some brains saturated the Renishaw inVia confocal microscope with the same measurement specifications that were optimal for the previous sample. So there was no consistency when obtaining the spectra. Those differences in the measurement not only affected the obtained luminescence but also the measurement time. For some samples, more than 6 hours separated the obtention of the first spectrum and the last, time during which the sample had ample time to suffer an even more extreme degradation.

With all that said, it cannot be stated the initial hypothesis to be invalid, but at the same time it is impossible to draw any conclusions. It became clear that it was first necessary to establish a strict measurement protocol if we wanted to obtain significant results. However, it is difficult to obtain brain tissue samples, and it was decided that it would be better to leave for the future this analysis and to focus in other, less delicate, fluorescent properties of the R6G-dyed brains.

That other propertie was the capacity (or lack of) of brain tissue to produce random laser. It was determined that, before doing that, a more careful mapping of the brain was necessary, keeping in mind the lessons learned in previous experiences. For RL a higher concentration of fluorophores is convenient, and it was decided that it would be better if the staining was made with R6G diluted in EtOH at 5mM, 10mM, 20mM and 50mM concentrations. The brains were now conserved in an ultrafreezer at a temperature of -80ºC and extracted just in time to proceed to the staining and measure-

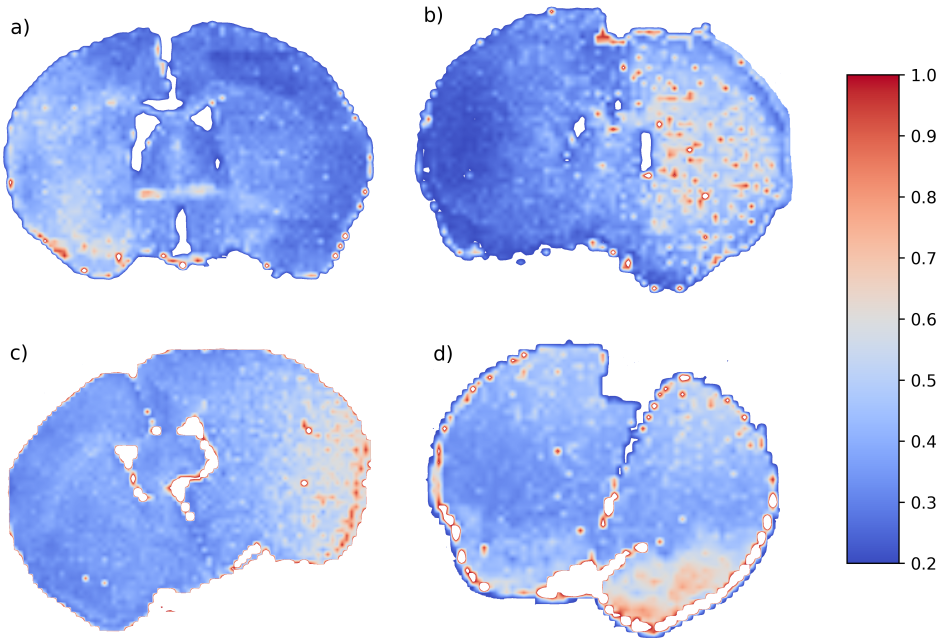

Figure 3.7: Normalized fluorescence intensity of mouse brain slices stained with R6G/EtOH with concentrations: **a)**5mM, **b)**10mM, **c)**20mM and **d)**50mM

ment. The bathing time was now the same for all samples, as described in section 2.1. The resulting maps can be seen in 3.7. The main conclusion we take from this set of mappings is that the distribution of R6G is fairly homogeneous for whatever staining dilution, beyond certain gradients that can be a consequence of the orientation of the brain while suspended in the bath.

3.2 Random Lasing

The first thing that needed to be done is to check that RL is possible within the brain. For that, a region of the stained brain was pumped with shots of increasing power in the same region of the brain, being always careful not to photobleach the sample. At some point of the increment of shot pump energy the typical broad spectrum of the R6G started to present narrow lines at some wavelengths. Those lines increased dramatically in intensity with slight increments of the pump power, becoming the dominant elements of the emission spectrum of the brain sample. Those characteristics describe what is known as **coherent random laser**. Once identified this emission as RL, it is inmediate to assign the energy at which it appears as the RL threshold. In figure 3.8 it is shown both identifying features for the 5mM-stained brain: the evolution of the spectrum and the peak emission intensity with increasing pump power.

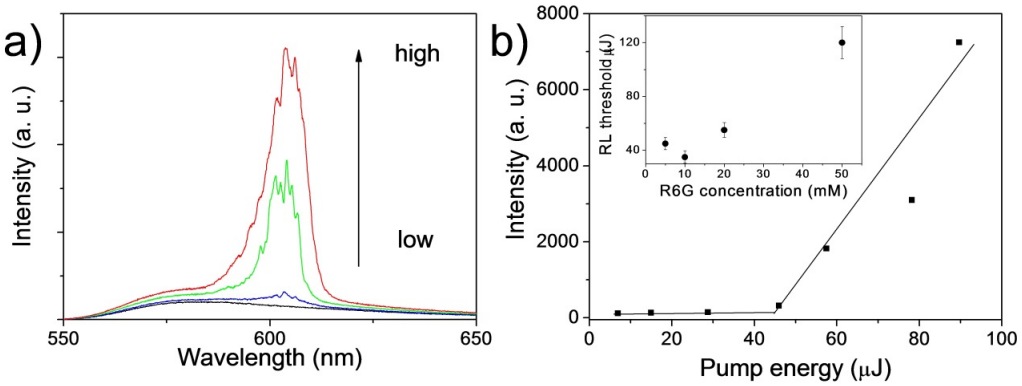

Figure 3.8: **a)** Random lasing spectra and **b)** emission intensity as a function of pump energy. The region excited was near the *corpus callosum* of the brain stained with 5mM R6G/EtOH. Inset shows RL threshold versus R6G impregnating concentration.

Figure 3.8.b lets us obtain the threshold for RL in that part of that brain: $45\mu J$. We proceeded to perform the same measurement and analysis for the brains stained at the other 3 concentrations. 10mM drove to a decrease in the threshold to only $35\mu J$, while for 20mM it was found to be $55\mu J$. The brain bathed in a 50mM R6G/EtOH dilution had the highest threshold by a wide margin: $120\mu J$. The initial increase in RL propensity (decrease in threshold) from dyeing with 5mM to 10mM dilution seems to be in conflict with the behaviour described for the fluorescence, where increasing the concentration to those levels produced a quenching of the emission. However, we have to keep in mind that we are not dealing with fluorescence now, but with RL. For RL to appear it must happen that, at some point, the luminosity gains exceed the losses: that can only happen if stimulated emission is produced. The 10mM brain has a higher proportion of dimers, that quench its total emission. But many of these are J-type, that is, emissive dimers, and we can see in table 3.1 that their τ_{av} is longer than the one for the monomers. This means that the electrons will spend more time in its excited state, and that increases the chances of stimulated emission.

Once we reach 20mM, however, the quenching due to the formation of higher-order aggregates is now too important to be offset by the higher average lifetime of dimers and the threshold starts increasing. This situation gets critical for the 50mM-stained brain, from which is very difficult to obtain RL without risking photobleaching.

3.2.1 RL intensity and threshold distribution

As has been stated in this work, the brain is a very heterogeneous organ. Simply opening a mouse brain atlas shows us its range of different distinguishable regions. This is why it makes sense to try to find differences in RL

behaviour between different regions of the brain, performing a ''pseudomapping". As the incident laser covers a big surface of the sample of the brain we cannot be very precise when selecting regions to analyse separatedly, but we can differentiate 4 main regions *Cortex, Corpus Callosum, Striatum* and *Amigdalar Cortex*, marked in figure 3.9.

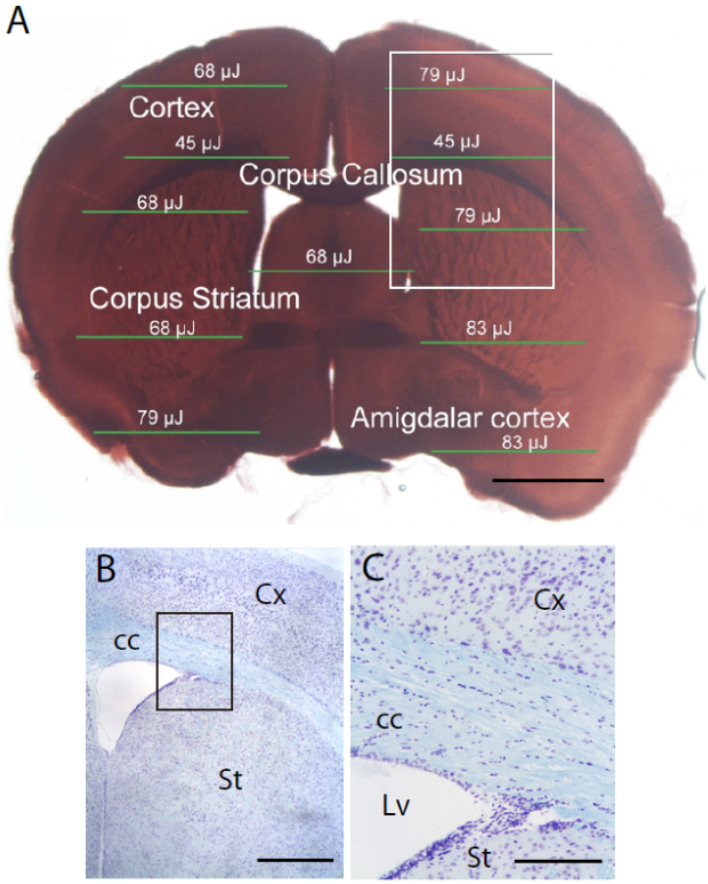

Figure 3.9: **A** shows the regions tested for RL. The green lines represent the excitation region, and the RL thresholds found are indicated. In panel **B**, as described in [10] *Kluver-Barrera staining of a brain region corresponding to the area indicated in A. Neurons are stained purple and myelinated axons (corpus callosum) are stained blue.* ***C****, high magnification microphotograph of area indicated in B, myelinated axons run parallel to section plane. cc, corpus callosum; Cx, cerebral cortex; Lv, lateral ventricle; St, corpus striatum.* The black bars are used as scale: the one in **A** represents 1.5 mm; Bar in **B**, 500 μm; Bar in **C**, 150 μm.

Said figure shows the regions pumped, where RL was obtained, and the threshold found in each one. To obtain this threshold the sample was shot with increasing pump laser intensity. The results of at least 5 shots were recorded for each energy (it is not named Random Laser just because: even when the conditions are optimal for its generation it could happen that no RL is produced). After analysing the results for each energy, by creating plots similar to the one in figure 3.8.b and by directly inspecting the spectra, the

threshold was determined. Most regions had their threshold around 70-80 μJ except for both *corpus callosum* shots, where it plummeted to only $45\mu J$. The rest of the brains (at different concentrations) had the same behaviour: homogeneous threshold values along all regions of the brain except for the *corpus callosum*.

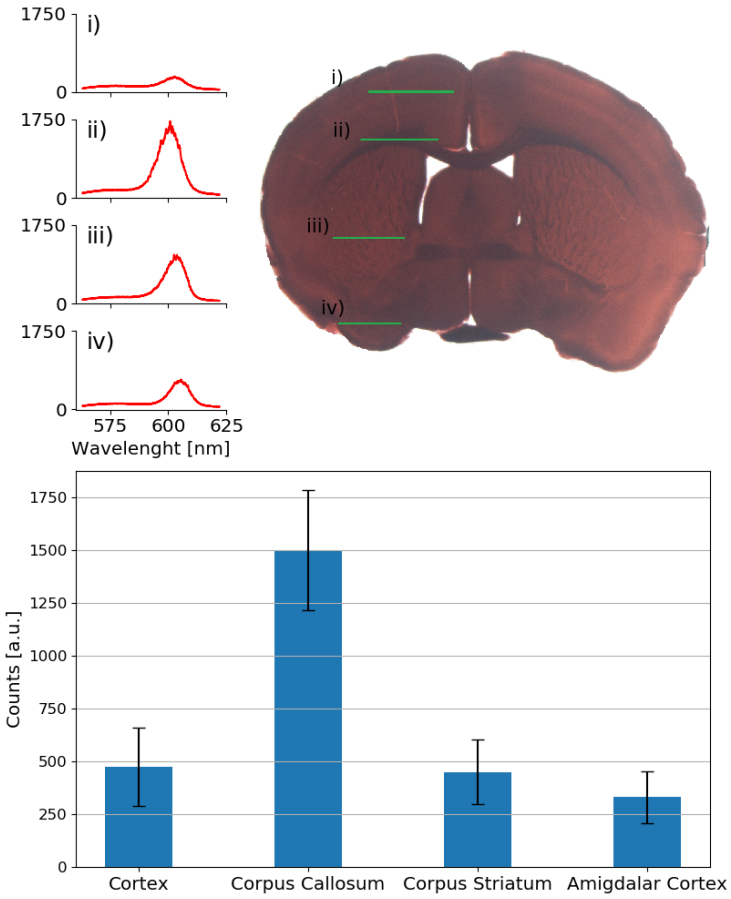

Figure 3.10: In the top panel we can see the different RL spectrums produced in each region under the same pump energy. The size of the image makes difficult to distinguish the narrow peaks that marks this as coherent RL, but they can be seen in the *corpus callosum* spectrum. The bottom panel shows the average peak intensity of the RL for each region and its standard deviation. This is the same brain represented in figure 3.9.

Once the threshold was determined, the pump energy was fixed at $158\mu J$ and several shots in the same four cerebral regions were taken, in order to study the variability of the intensity of the RL (that was almost sure to happen, since the pump energy is far beyond the threshold). The results are presented in figure 3.10. Once again, RL only really differs in the *corpus callosum*, where it is far more intense. The second most intense RL was found in the *striatum*.

We have found a more intense RL, and more easily obteined, in the *corpus callosum*. There can be a phisiological reason for this, and it probably does

not have any relation with different afinnity to R6G, as 3.7 showed that the distribution of R6G was fairly homogeneous. Two things define a RL: a gain medium and scattering centres. If a medium has stronger fluorescence it will be easier to see RL in it: similarly, greater scattering strength will have the same effect. In this case we have seen that the gain capacity of the medium does not change from region to region: the explanation for the higher probability of RL in the *corpus callosum* must lay in its scattering strength. We have already described the composition of this region: it is a very lipidic environment of ''fibres" that go from one hemisphere to the other. The lipidic nature of this region increases its refractive index [15], which in turn increases light scattering. There are intersticial spaces filled with aqueous substances, for which the contrast in n is higher if the adjacent medium is lipidic, and that is one reason why the scattering is more efficient in this region. But perhaps the actual spatial distribution of the fibres is more important: they run parallel among them, conforming a non-isotropic environment, as can be seen in panel b of figure 3.9. This dramatically increases the scattering strength of the region. The *striatum* also has a high percentage of lipidic regions, and perhaps that is why RL intensity there is the second highest, but it is much more isotropic than the *corpus callosum*, and that proves to be of the utmost importance. It would be interesting to perform the same experiment in longitudinal slices, instead of transversal.

3.2.2 Fourier analysis and cavity size determination

As seen in the introduction, coherent random laser produces different modes, each one associated with a different ''cavity" (or more accurately, closed optical path). Through Fourier analysis of the spectrum we can find those modes and, assuming a value of the refractive index, calculate the length of those paths. This would give us information about the distribution of scattering centres on the excited region: that is, structural information about the tissue. The samples were thicker than the ones used when dyeing the fluorescent emission of stained brains. We now had brains $200\mu m$ thick. This thickness facilitated the manipulation of the brain slices, but it was also necessary to discard effects steeming from light crossing the sample. After all, we can expect to need very high intensities in order to obtain RL. For each shot that produced RL we need to perform a Fourier transform (after changing the independent variable, or sampling variable, to the wavenumber k in μm^{-1}) and to inspect the modes found. This process is shown in figure 3.11. Some of them are artifacts from the finite size of the signal, but those are consistent from one spectrum to the other, and therefore are easily filtered. After performing this analysis for all shots in the different regions, a histogram of cavity sizes was found for each region. It can be seen in figure 3.12. The cavity sizes were obtained using the equation $p_m = m\frac{L_C n}{\pi}$, already described in section 1.2, where n was assumed to be 1.4 [16], above the refractive index of water.

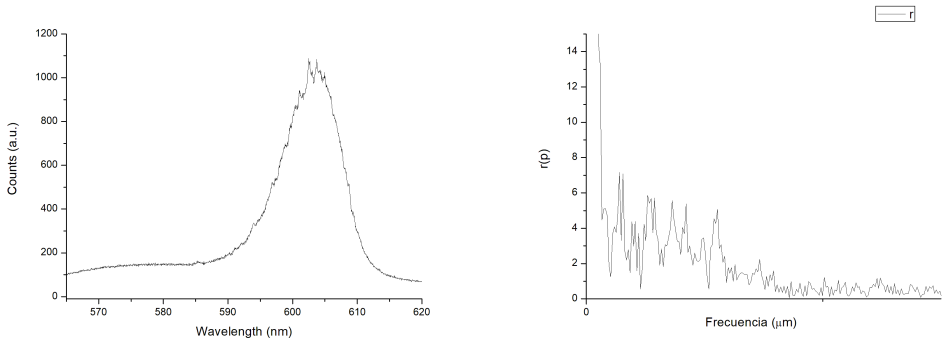

(a) $I(\lambda)$ (b) Results of the Fourier analysis

Figure 3.11: In the left panel an intense coherent RL signal is shown. To its right, the $|\mathcal{F}[I(k)]|$ is plotted against μm

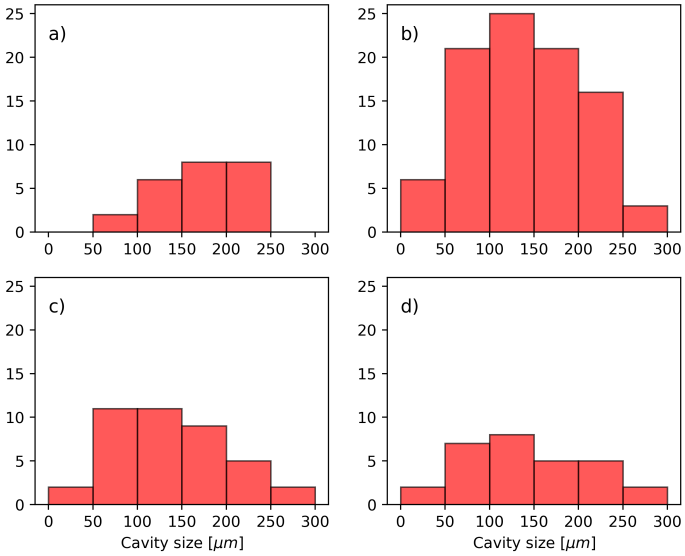

Figure 3.12: Histogram of cavity sizes found viathe Fourier analysis of the obtained coherent RL in **a)** *cortex*, **b)** *corpus callosum*, **c)** *striatum* and **d)** *amigdalar cortex*.

From this data we determined the average length of the closed optical paths to be:

Region	$\langle L_C \rangle [\mu m]$	$\sigma_{L_C} [\mu m]$
Cortex	165.3	44.2
Corpus Callosum	140	59.8
Striatum	136.2	63.3
Amigdalar Cortex	141.5	60.0

The main takeaway from this analysis should be that the data is insufficient. Even though we are beyond the threshold we do not see RL with every shot, specially in zones outside the *corpus callosum*. The pump energy had to be the same for every zone, lest we introduce error sources in the comparison, so an energy that was well beyond the *CC* threshold was not as effective outside it. If this energy had increased, there was a risk of photobleaching the sample or even damaging the tissue, so it was decided to err on the side of precaution and use the lower energy. This meant that not all shots produced RL, and those shots that did not always resolved the coherent RL as well as it is necessary for the Fourier analysis. An example of a well-defined coherent RL spectra and the result of performing the Fourier transform on it is shown in figure 3.11.

Not only were some shots unsuccessful, but also there were only five shots per zone measured (in both hemispheres), which also reduced the amount of data. A greater number of measurements would have had two positive consequences: with more data it is possible to perform more accurate statistics: we see that the σ's for the cavity sizes are too large, almost half of the mean value in 3 out of the 4 regions. That forces us to not take the $\langle L_C \rangle$ at face value, a decision that could have been made just by looking at the shape of the histograms. Apart from that, more measurements would have allowed us to filter spurious modes from the Fourier transform and the real sizes of the cavities would have been more clear. With the results obtained, it would be difficult to draw any conclusions.

3.3 Fabry-Perot cavities

As was said in section 1.3, a etalon or Fabry-Perot resonator can be used to determine the refractive index of the media inside a resonant cavity by analysing an interference pattern superimposed on the normal spectra of a sample. In this case, we do not have a simple cavity, but one with a brain slice in it. This means that equations 1.2 and 1.3 take another form, taking into account that the light is passing through two different mediums:

$$m\lambda_m = 2(n_1 d_1 + n_2 d_2) \tag{3.4}$$

$$FSR = |\lambda_{m-1} - \lambda_m| = \frac{\lambda_m}{2(n_1 d_1 + n_2 d_2)} \tag{3.5}$$

In this case, n_1 and d_1 refer to the refractive index of whatever surrounds the brain (it will change depending on the sample) and the space not filled by the slice. n_2 **and** d_2 **are, therefore, the refractive index and thickness of the brain sample**. In all cases, d_2 is assumed to be constant with a value of $60\mu m$. The samples have to be thin: the light must cross it entirely at least two times, and if it were too thick the absorption and dispersion would be too big and we would not have any signal to detect. We have to

remember that the resonator is composed of two parallel mirrors: the light that manages to escape is but a fraction of the light generated. Any extra loss has a big impact.

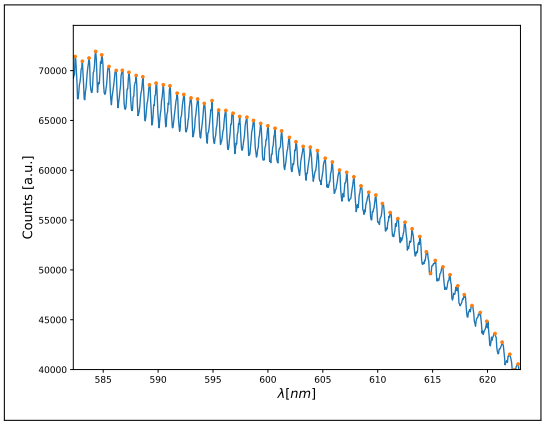

Figure 3.13: Fluorescent spectra from a dilution of R6G/glycerol inside a Fabry-Perot cavity.The software-identified peaks are marked with orange points.

The first task was to determine the best measurement protocol. First an appropiate cavity was needed. Two one-sided coated glasses were used at first: by introducing measured plastic separators between them a cavity was formed inside which the brain tissue could be placed. The first issue appeared here, since the size of the cavity appeared to be bigger than the separators would allow. The thickness of those separators was measured using a mechanical sensor: but this sensor inflicted a pressure on the plastic separators that could not be matched by the very light mirrors, so they deformed and changed the size of the cavity, making it inhomogeneous. We attempted to add weights to the setup, but it interfered with the conduction of the measurements and was not optimal. The solution was to use another pair of mirrors with a built-in, reliable separator. The cavity formed in this device was bigger than before: from $50\mu m$ to $170\mu m$. In the first case, we hoped that the brain would take up the entirety of the cavity, making unnnecessary to take into account the media. With this new etalon we would have to be more careful and introduce the medium of the cavity as another factor of our analysis and setup.

Several attempts with R6G-dyed brains were performed, adding also a glycerol or water drop to not have air as the medium inside the cavity. No matter the combination, the results were extremely noisy for points inside the brain. Data manipulation was difficult and almost pointless: there was no means to separate the interference-induced peaks from the noise of the signal. Analysing the spectra one by one was not an option: the mapping was performed with a resolution of $100\mu m$ in both the x and y-axis: this meant that each mapping had more than two thousand individual spectrums to study. We tried using non-stained brains with a drop of R6G/PBS and R6G/glycerol dilution on top to act as an optical medium. This generated a signal that was both tractable and obtainable in a reasonable time. An example of the signals obtained can be seen in the top panels of figures 3.14 (outside the brain) and 3.15 (inside the brain).

Once a good signal was obtained a mapping was performed. After this, the treatment of the data came to be the main issue of this part of the work. First we needed to indentify the peaks associated with the etalon. While that

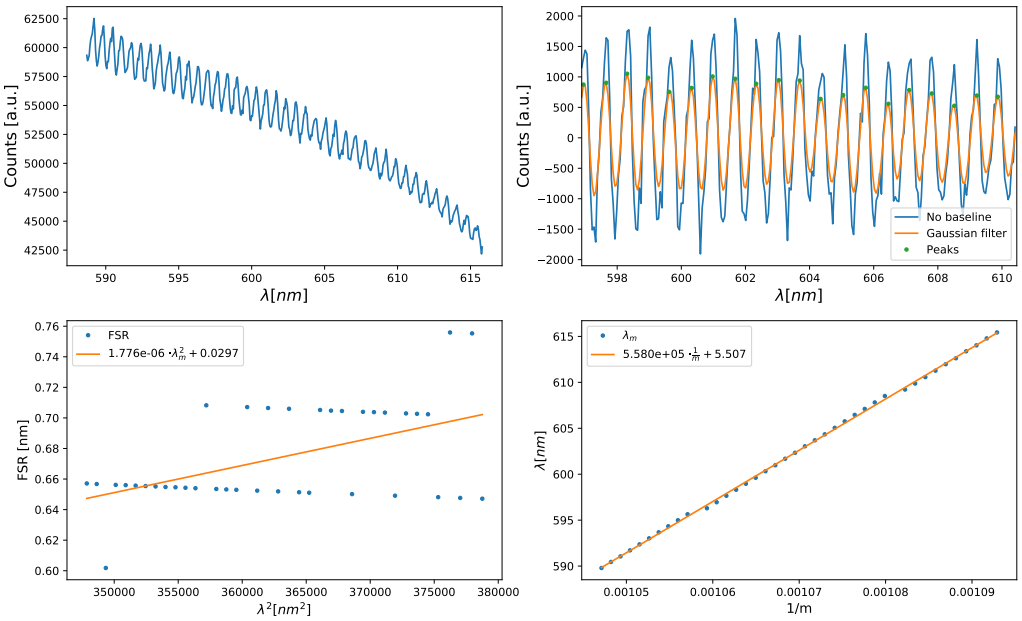

Figure 3.14: Signal and treatment of that signal from **outside** the brain. Top panels: obtained spectrum on the left, after treatment on the right. This last panel is a enhanced region of the entire spectrum showed on the left. Bottom panels: FSR against λ^2 and λ against $1/m$; both plots also show the linear regression calculated.

could be easily done for the points outside the brain without manipulating the data (see figure 3.13), when the light had to cross the signal received was noisier (the example in fig. 3.15 is one of the best signals obtained inside the brain). This meant that the spectra had to be treated. First, the baseline was extracted. The spectrum was fitted to a 5^{th} order polynomial and that fit was substracted from the signal. Then a gaussian filter was applied. To determine the optimal widths of the gaussian wavelets expected, a range of FSRs was calculated from the possible n that can be expected (in the case of points outside the brain this is not actually necessary, as there is a fixed and known refractive index). After the gaussian filter is applied to the signal, we expect that the only peaks that remain are the interference-created ones, having eliminated much of the noise. With this treated ignal it is far easier to identify the peaks. We can see the results of this treatment on noisy signals in figure 3.15.

Once the peaks are obtained, the FSR is calculated and a linear fit of this FSR against λ^2 gives us an approximation to $1/(2n_1d_1)$ or $1/[2(n_1d_1+n_2d_2)]$, depending on the position of the measurement. We do not use this value to calculate any n, but to approximate the value of m for each λ. Both values are connected in eq. 1.2. Now we can plot λ against $1/m$: the slope of the line of fit is equal to $2n_1d_1$ (or $2(n_1d_1 + n_2d_2)$ for light that went through the brain). The first step of this proccess is shown in the bottom-left panels

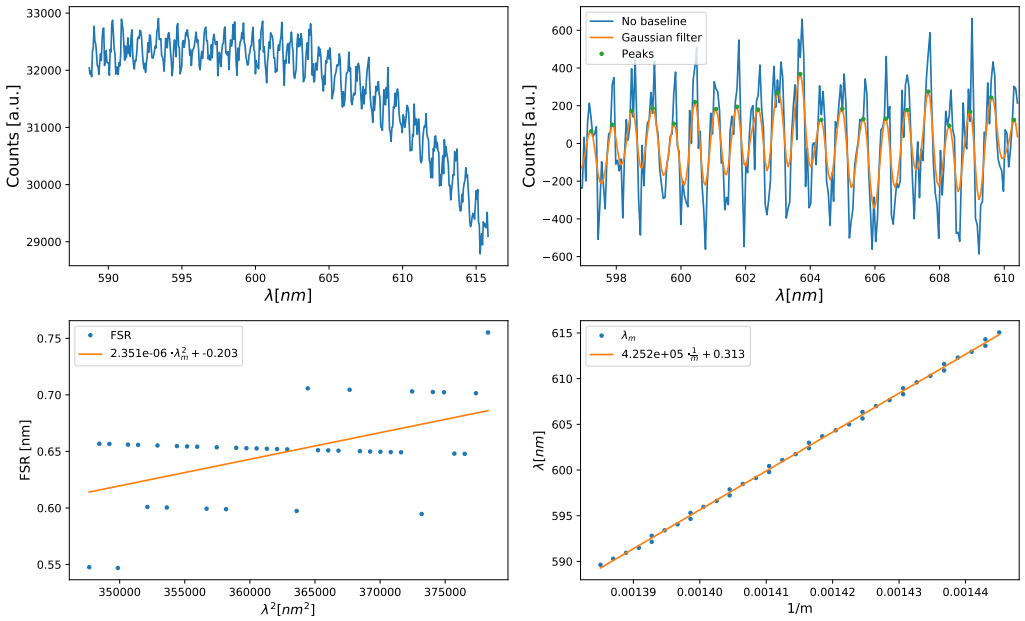

Figure 3.15: Signal and treatment of that signal from **inside** the brain. Top panels: obtained spectrum on the left, after treatment on the right. This last panel is a enhanced region of the entire spectrum showed on the left. Bottom panels: FSR against λ^2 and λ against $1/m$; both plots also show the linear regression calculated.

of figures 3.14 and 3.15. The bottom-right panels correspond to the second part.

What we do with this data differs depending on the presence or not of the brain. For points outside the brain we assume a refractive index ($n_1 = 1.33$ for water, $n_1 = 1.4718$ for glycerol) and calculate d. After doing so, the idea was to interpolate the values found to the points inside the brain: that way we could find the size of the cavity at each point, and with that and knowing that $d_2 = 60\mu m$, calculate d_1. We would use those d values to calculate n_2. However, the values of d varied too much from point to point, a consequence of the finesse of the treatment or the quality of the signal. In any case, the thickness was found to be, on average, $190\mu m$, with a, error of $\pm 20\mu m$. This significant error affected the precision of the values of n obtained.

Now we can obtain the maps of n_2 for the entire sample. The results of this calculation are shown in figures

The first thing one has to notice is that the glycerol, due to its viscosity, has not covered the entire cavity. This hinders the entire analysis, since we have now three different zones with different composition and refractive index, with not way of knowing *a priori* which one to use. We should focus on the sample treated with a drop of R6G/H_2O. The mappings are not as accurate as we expected. At many points, it differs significantly from the expected values (see [16] for an approximate idea) It also has a high variability: it

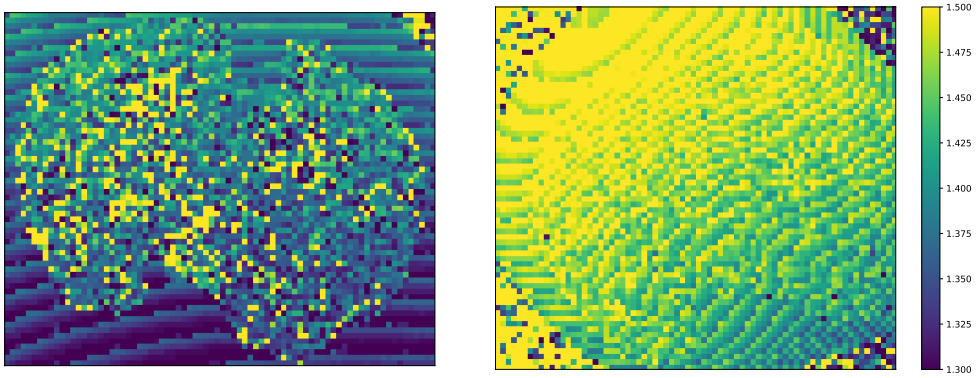

(a) Optical medium: R6G/H_2O

(b) Optical medium: R6G/Glycerol

Figure 3.16: Both figures share the same color scale, starting at $n = 1.33$ and ending in $n = 1.5$. Values outside this range are not possible for the samples studied.

is not only physically unexpected: it also means that the resolution used is not enough detailed to differentiate structures of the brain. There can be several explanations for this results: the first are, obviously, experimental sources of error. The distribution of the drop might be uneven; the brain can be not uniforms and thus d_2 differ from one point to the other; the signal can still be too weak to properly analise... Second we have to study the accuracy of the numerical treatment of data. Slight departures from the desired values in each of the steps of the process can have important effects on the final result. Skipping a value of the FSR, identifying as a peak an artifact from the noise, making a mistake on the approximation of just one value of m... All those mistakes can ruin the entire chain of calculations. Although no appreciable mistake has been found, the fact is that each mapping is comprised of thousands of spectra, which forces us to automatize the process. This makes troubleshooting more difficult and we cannot assure that there is no bug in the code. Lastly, some assumptions about the behaviour of the interferometer can be wrong. The brain has a high extintion coefficient (it is not transparent to incident radiation) and therefore it is difficult to assert that it presents enough finesse to aplly the equations presented here (citesaleh). More importantly, the brain, as most biological tissues, has an appreciable scattering strength (as we saw in section 3.2). This means that the light rays we detect may not have followed a trajectory perpendicular to the mirrors, which would render pointless the entire interferometre approach to the problem. Further test would be needed to explore all these sources of error, the most pressing one being the last presented. The only takeaway we can have is that those test should be performed adding a single drop of R6G/H_2O on top of an unstained brain.

4 Conclusions

This work has provided a great opportunity to introduce us to the handling and measurement of biological samples as frail as brain slices. The project was comprised of three different areas of study: fluorescence emission studies of the brain, Random Laser obtention in the brain and mapping of the refractive index of the brain using Fabry-Perot resonators. The conclusions drawn for each of these are presented now:

- Fluorescence spectra of R6G dilutions has two different regimes: for low concentrations, 1μM to 1mM, the emission is dominated by monomers, while the fraction of dimers grows gradually, slightly redshifting the spectra. When we reach high enough concentrations (5-50mM) the redshift stops, but the increasing number of dimers produce an overall decay of the lifetimes of the monomers, since there are now mechanisms of energy transfer between monomers and higher order aggregates. However, those aggregates still do not have a noticeably role in the emission spectra position: only in its intensity.

  Once R6G is staining the tissues instead of suspended in solution, the picture changes dramatically. For the higer concentrations (5-50mM) the emission is now dominated by the J-dimers: monomers are barely emissive, since most of the energy of the excited ones ends up being tranfered non-radiatively to the dimers and higher order aggregates. Those last compounds of R6G are not very emissive, but there are enough of them to alter and widen the spectrum. The decay of the emission is also more complex now, since there are many emission mechanism acting at the same time. In order to fit the decays we have needed to assume at least 4 different exponentials, with which we have calculated an average lifetime for two different wavelengths, 580 nm and 620nm. The different τ_{av} at each wavelength indicates that the centers responsible for the emission are not the same across the spectrum.The first τ_{av} is around half the second one for all concentrations.

  The emission of brains stained with R6G dilutions do not show discernible common patterns. This may be due to the inconsistency in the preparation of the samples: all the brains were bathed with 1mM or 10mM R6G dilutions, and we have seen that the behaviour of the emission in those two concentration ranges vary greatly. Perhaps be-

cause the 1mM dilution do not provide a favorable environment for the formation of dimers *before* being in contact with the brain, samples stained with said dilution exhibited an emission dominated by monomers, where higher R6G concentrations meant higher emission, while other brains did not show this correlation. There was indications of differential behaviour from the *corpus callosum*, but the differences from one map to the other were too great to draw any conclusions. Since there were no common characteristics among WT brains, it was impossible to find any diffentiation factors between WT brains and the ones suffering from AD.

- Coherent RL was succesfully obtained in brain tissue stained with R6G/EtOH dilutions with concentrations ranging 5mM to 50mM. The characteristics of the RL depended on both the concentration of dye and the estimulated region of the brain slices. The concentration most favorable for the RL was found to be 10mM, with a minimal threshold of $35\mu J$ in the *corpus callosum*. The rest of the the brain exhibited thresholds around 60-80μJ. This region, *corpus callosum*, exhibited the lowest threshold in all the samples studied. Not only that but the RL obtained there was always the more intense. Since the fluorescence emission of this region did not have significant differences from the rest of the brain, these differences in RL probability and intensity have to relate to the scattering strength of the medium. The configuration of this region (long lipidic fybrils, parallel to one another and parallel to the rectangular exciting beam) and its composition (high lipid concentration that creates higher n contrast) explains the increase in scattering strength compared to the rest of the brain. It would be interesting to analise this region in longitudinal cuts of the brain, instead of transversal. In conclusion, RL is not only achievable in brain tissue, it can also be used to find microstructural characteristics of the tissue, as well as its composition.A more complete study, in the sense of one with a bigger number of experiments, samples and measurements, could allow us to fine-tune the interpretation of the obtained RL and could even prove useful as a diagnostic tool. The Fourier analysis of the coherent RL modes allowed us to calculate the length of a number of closed optical paths (optical cavities in the tissue), ranging mainly between $60\mu m$ and $200\mu m$, being the most common cavities around $140\mu m$ long. An increased number of experiments would allow us to perform an analysis of true statistical significance, which would be very helpful in any possible application of RL phenomena in brain tissue.

- A Fabry-Perot resonator containing a slice of brain tissue was succesfully built using two one-sided mirrors with a built-in separator that formed a cavity with a size of around $170\mu m$. This size could vary when a fluid was introduced in the cavity. The introduction of the fluid was

a result of the signal optimization process. It was found that, in order to obtain a readable signal, the sample had to remain unstained, and the optical gain medium had to be added in form of a drop of R6G diluted in water or glycerol. Water was preferred since its lower viscosity meant that the drop covered the entire mapping region. The lower solubility of R6G in water also helped to differentiate between regions outside and inside the brain.

The etalon allowed us to calculate the thickness of the cavity at each point and map the refractive index across the brain slice. We found a great uncertainty in the values of d (cavity size), that resulted in unreliable values of n. Further improvements in the experimental methodology should provide us more accurate values of the refractive index.

The first two objetives of this Master's Thesis were succesfully reached. A technique for the mapping of fluorescence in brain slices was developed, technique that could easily be adapted to different samples. RL was obtained in brain tissue for the first time (as of today, I have not found any reports of this phenomena), and the results indicate that, with further work, it could be used as a diagnostic and characterization tool. The last area of work, the determination of the refractive index across the brain using a Fabry-Perot resonator, still needs a more comprehensive treatment, since there is still a great degree of uncertainty in the results obtained.

A Fluorescence mappings of the rest of samples

In this appendix the results of the succesfully mapped mouse brain samples are presented, along with the respective staining process for each one. The differences between them are thus made clear.

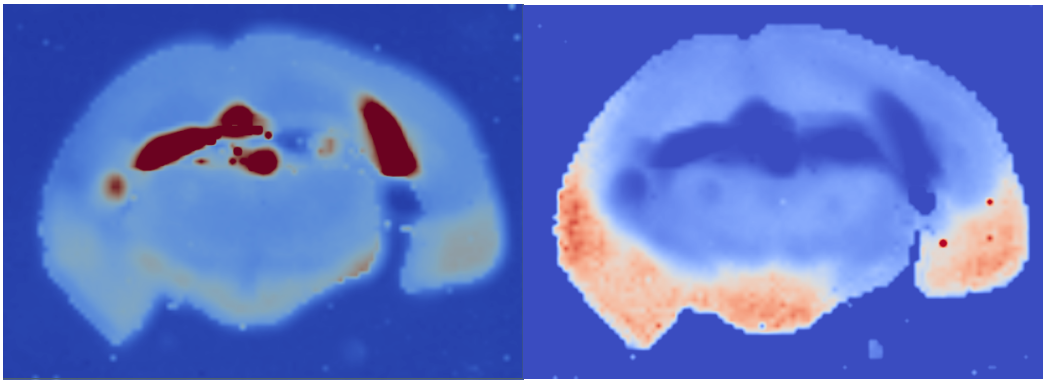

(a) Normalized intensity (b) I_{615}/I_{570}

Figure A.1: WT brain, bathed in 10mM R6G/PBS for 24h. The maximum value of I_{615}/I_{570} (color red) is 7.

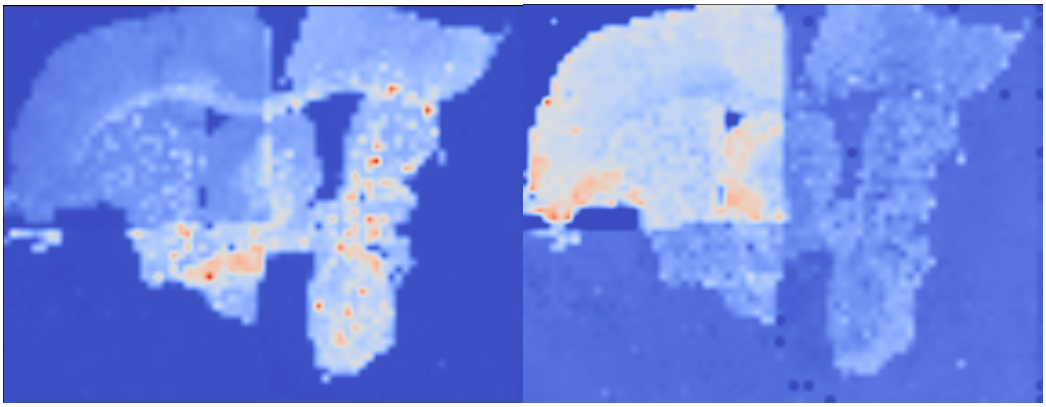

(a) Normalized intensity (b) I_{615}/I_{570}

Figure A.2: AD brain, bathed in 10mM R6G/PBS for 20h. Badly damaged during manipulation. The maximum value of I_{615}/I_{570} (color red) is 7. We can appreciate the higher intensity of emission in the *corpus callosum*. This brain comes from the same litter than A.1.

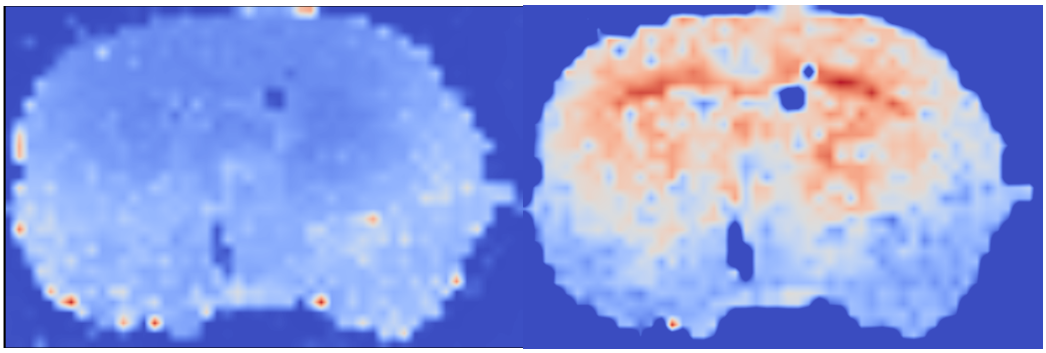

(a) Normalized intensity (b) I_{615}/I_{570}

Figure A.3: AD brain, bathed in 50mM R6G/EtOH for 18h. The maximum value of I_{615}/I_{570} (color red) is 1.2. Note chance in concentration and solvent when comparing with the rest of the samples.

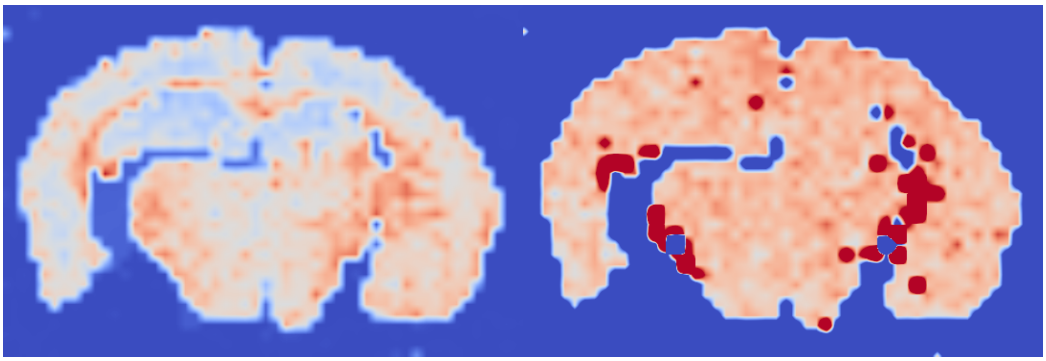

(a) Normalized intensity (b) I_{615}/I_{570}

Figure A.4: AD brain, bathed in 1mM R6G/PBS for 20h. The maximum value of I_{615}/I_{570} (color red) is 0.5.

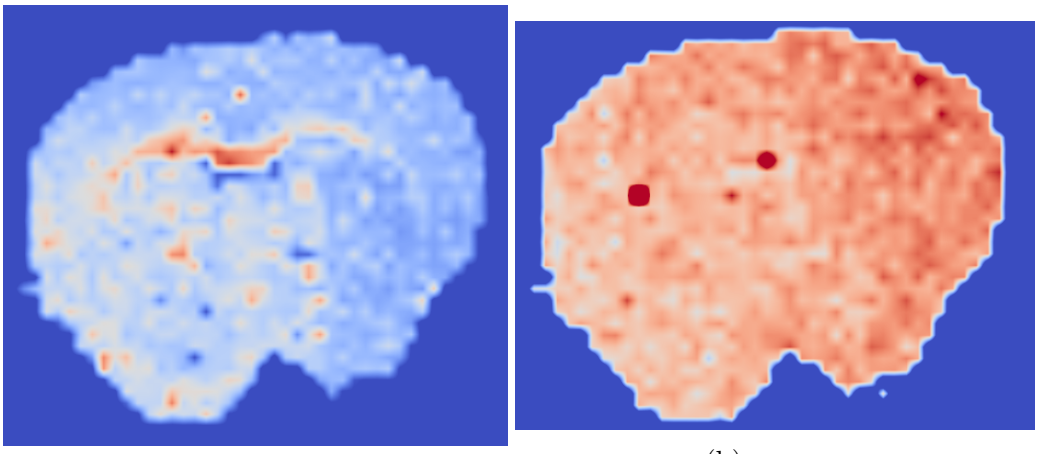

(a) Normalized intensity

(b) I_{615}/I_{570}

Figure A.5: WT brain, bathed in 1mM R6G/PBS for 20h. The maximum value of I_{615}/I_{570} (color red) is 0.5. Same staining process as in A.4, which is also from a sibling of this mouse.

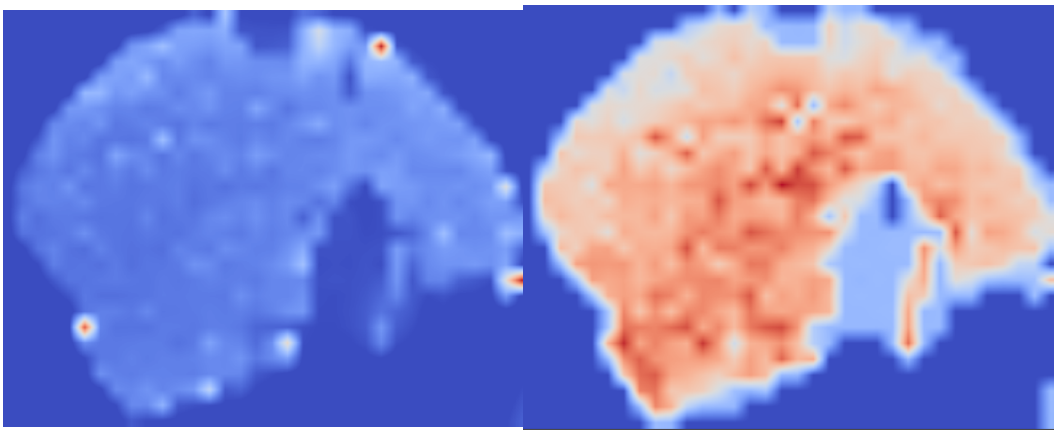

(a) Normalized intensity

(b) I_{615}/I_{570}

Figure A.6: WT brain, bathed in 10mM R6G/PBS for 1h. The maximum value of I_{615}/I_{570} (color red) is 1.3. The sample remained in a water bath for the duration of the experiment. Some of the R6G impregnating the bain diluted in this bath, masking the signal.

Bibliography

[1] Joseph R. Lakowicz *Principles of Fluorescence Spectroscopy*, third edition. Springer Science+Bussiness Media, New York, 2006.

[2] Bahaa E. A. Saleh, Malvin Carl Teich *Fundamentals of Photonics* John Wiley & Sons, Inc, 1991

[3] Diederik S. Wiersma *The physics and applications of random lasers* Nature Physics volume 4, pages 359–367 (2008)

[4] Marta Urgellés Barcala *Estudio de fluorescencia en aplicaciones bilógicas* TFM, máster en Técnicas de I+D+i para Ciencias e Ingeniería, ULL, 2016

[5] R. W. Sabnis *Handbook of Fluorescent Dyes and Probes* John Wiley & Sons, 2015

[6] C.On, E.K. Tanyi, E. Harrison and M.A. Noginov. *Effect of molecular concentration on spectroscopic properties of poly(methyl methacrylate) thin films doped with rhodamine 6G dye* Optical Materials Express, 2017

[7] P. Hanczyc, L. Sznitko, C. Zhong and Alan J. Heeger. *Stimulated Emission from Rhodamine 6G Aggregates Self- Assembled on Amyloid Protein Fibrils* ACS Photonics 2015, 2, 1755-1762

[8] A. J. Musser, *et al. Intermolecular states in organic dye dispersions: excimers vs. aggregates* J. Mater. Chem. C, 2017, 5, 8380

[9] Randal C. Polson and Z. Valy Vardeny *Random lasing in human tissues* Applied Physics Letters 85, 1289 (2004); doi: 10.1063/1.1782259

[10] F. Lahoz, A. Acebes, T. González-Hernández, S. de Armas-Rillo, K. Soler-Carracedo *et al. Random lasing in brain tissue* Sent to Organic Electronics, publishing pending.

[11] S. Terdale, A. Tantray. *Spectroscopic study of the dimerization of rhodamine 6G in water and different organic solvents* J. Mol. Liq. 225 (2017) 662-671. doi:10.1016/j.molliq.2016.10.090.

[12] A. Penzkofer, W. Leupacher *Fluorescence behaviour of highly concentrated rhodamine 6G solutions* J. Lumin. 37 (1987) 61-72. DOIi:10.1016/0022-2313(87)90167-0.

[13] V. Martínez Martínez, F. López Arbeloa, J. Bañuelos Prieto, I. López Arbeloa *Characterization of Rhodamine 6G Aggregates Intercalated in Solid Thin Films of Laponite Clay* 2 Fluorescence Spectroscopy, J. Phys. Chem. B. 109 (2005) 7443–7450. DOI:10.1021/jp050440i.

[14] Piotr Hanczyc, Lech Sznitko, Chengmei Zhong and Alan J. Heeger *Stimulated Emission from Rhodamine 6G Aggregates Self-Assembled on Amyloid Protein Fibrils* ACS Photonics 2015, 2, 1755-1762. DOI: 10.1021/acsphotonics.5b00458

[15] J. Sun, S.J. Lee, L. Wu, M. Sarntinoranont, H. Xie *Refractive index measurement of acute rat brain tissue slices using optical coherence tomography* Opt. Express. 20 (2012) 1084. DOI:10.1364/OE.20.001084.

[16] Jonas Binding, Juliette Ben Arous, Jean-François Léger, Sylvain Gigan, Claude Boccara and Laurent Bourdieu *Brain refractive index measured in vivo with high-NA defocus-corrected full-field OCT and consequences for two-photon microscopy* Opt. Express 20, 1084-1095 (2012)

[17] Risacher S.L., Anderson W.H., Charil A., Castelluccio P.F., Shcherbinin S., Saykin A.J., Schwarz A.J. *Alzheimer disease brain atrophy subtypes are associated with cognition and rate of decline.* Neurology. 2017 Nov 21;89(21):2176-2186. doi: 10.1212/WNL.0000000000004670

[18] Wahlund L.O. *Magnetic resonance imaging and computed tomography in Alzheimer's disease.* Acta Neurol Scand Suppl. 1996;168:50-3.